Neutron-proton scattering in the context of the *d**(2380) resonance

P. Adlarson,[1] W. Augustyniak,[2] W. Bardan,[3] M. Bashkanov,[4,5] F. S. Bergmann,[6] M. Berłowski,[7] H. Bhatt,[8] M. Büscher,[9,10]
H. Calén,[1] I. Ciepał,[3] H. Clement,[4,5,*] D. Coderre,[11,12,13,†] E. Czerwiński,[3] K. Demmich,[6] E. Doroshkevich,[4,5] R. Engels,[11,12]
A. Erven,[14,12] W. Erven,[14,12] W. Eyrich,[15] P. Fedorets,[11,12,16] K. Föhl,[17] K. Fransson,[1] F. Goldenbaum,[11,12] P. Goslawski,[6]
A. Goswami,[11,12,18] K. Grigoryev,[12,19,20] C.-O. Gullström,[1] F. Hauenstein,[15] L. Heijkenskjöld,[1] V. Hejny,[11,12] M. Hodana,[3]
B. Höistad,[1] N. Hüsken,[6] A. Jany,[3] B. R. Jany,[3] L. Jarczyk,[3] T. Johansson,[1] B. Kamys,[3] G. Kemmerling,[14,12] F. A. Khan,[11,12]
A. Khoukaz,[6] D. A. Kirillov,[21] S. Kistryn,[3] H. Kleines,[14,12] B. Kłos,[22] W. Krapp,[15] W. Krzemień,[3] P. Kulessa,[23] A. Kupść,[1,7]
K. Lalwani,[8,‡] D. Lersch,[11,12] B. Lorentz,[11,12] A. Magiera,[3] R. Maier,[11,12] P. Marciniewski,[1] B. Mariański,[2]
M. Mikirtychiants,[11,12,13,20] H.-P. Morsch,[2] P. Moskal,[3] H. Ohm,[11,12] I. Ozerianska,[3] E. Perez del Rio,[4,5] N. M. Piskunov,[21]
P. Podkopał,[3] D. Prasuhn,[11,12] A. Pricking,[4,5] D. Pszczel,[1,7] K. Pysz,[23] A. Pyszniak,[1,3] C. F. Redmer,[1,§] J. Ritman,[11,12,13]
A. Roy,[18] Z. Rudy,[3] S. Sawant,[8,11,12] S. Schadmand,[11,12] T. Sefzick,[11,12] V. Serdyuk,[11,12] V. Serdyuk,[11,12,24] R. Siudak,[23]
T. Skorodko,[4,5,25] M. Skurzok,[3] J. Smyrski,[3] V. Sopov,[16] R. Stassen,[11,12] J. Stepaniak,[7] E. Stephan,[22] G. Sterzenbach,[11,12]
H. Stockhorst,[11,12] H. Ströher,[11,12] A. Szczurek,[23] A. Täschner,[6] A. Trzciński,[2] R. Varma,[8] G. J. Wagner,[4,5] M. Wolke,[1]
A. Wrońska,[3] P. Wüstner,[14,12] P. Wurm,[11,12] A. Yamamoto,[26] L. Yurev,[24,‖] J. Zabierowski,[27] M. J. Zieliński,[3] A. Zink,[15]
J. Złomańczuk,[1] P. Żuprański,[2] and M. Żurek[11,12]
(WASA-at-COSY Collaboration)

R. L. Workman,[28] W. J. Briscoe,[28] and I. I. Strakovsky[28]
(SAID Data Analysis Center)

[1]*Division of Nuclear Physics, Department of Physics and Astronomy, Uppsala University, Box 516, 75120 Uppsala, Sweden*
[2]*Department of Nuclear Physics, National Centre for Nuclear Research, ul. Hoza 69, 00-681, Warsaw, Poland*
[3]*Institute of Physics, Jagiellonian University, ul. Reymonta 4, 30-059 Kraków, Poland*
[4]*Physikalisches Institut, Eberhard-Karls-Universität Tübingen, Auf der Morgenstelle 14, 72076 Tübingen, Germany*
[5]*Kepler Center for Astro and Particle Physics, University of Tübingen, Auf der Morgenstelle 14, 72076 Tübingen, Germany*
[6]*Institut für Kernphysik, Westfälische Wilhelms-Universität Münster, Wilhelm-Klemm-Str. 9, 48149 Münster, Germany*
[7]*High Energy Physics Department, National Centre for Nuclear Research, ul. Hoza 69, 00-681, Warsaw, Poland*
[8]*Department of Physics, Indian Institute of Technology Bombay, Powai, Mumbai-400076, Maharashtra, India*
[9]*Peter Grünberg Institut, Forschungszentrum Jülich, 52425 Jülich, Germany*
[10]*Institut für Laser- und Plasmaphysik, Heinrich-Heine Universität Düsseldorf, 40225 Düsseldorf, Germany*
[11]*Institut für Kernphysik, Forschungszentrum Jülich, 52425 Jülich, Germany*
[12]*Jülich Center for Hadron Physics, Forschungszentrum Jülich, 52425 Jülich, Germany*
[13]*Institut für Experimentalphysik I, Ruhr-Universität Bochum, Universitätsstr. 150, 44780 Bochum, Germany*
[14]*Zentralinstitut für Engineering, Elektronik und Analytik, Forschungszentrum Jülich, 52425 Jülich, Germany*
[15]*Physikalisches Institut, Friedrich-Alexander-Universität Erlangen-Nürnberg, Erwin-Rommel-Str. 1, 91058 Erlangen, Germany*
[16]*Institute for Theoretical and Experimental Physics, State Scientific Center of the Russian Federation,*
Bolshaya Cheremushkinskaya 25, 117218 Moscow, Russia
[17]*II. Physikalisches Institut, Justus-Liebig-Universität Gießen, Heinrich-Buff-Ring 16, 35392 Giessen, Germany*
[18]*Department of Physics, Indian Institute of Technology Indore, Khandwa Road, Indore-452017, Madhya Pradesh, India*
[19]*III. Physikalisches Institut B, Physikzentrum, RWTH Aachen, 52056 Aachen, Germany*
[20]*High Energy Physics Division, Petersburg Nuclear Physics Institute, Orlova Rosha 2, Gatchina, Leningrad 188300, Russia*
[21]*Veksler and Baldin Laboratory of High Energiy Physics, Joint Institute for Nuclear Physics, Joliot-Curie 6, 141980 Dubna, Russia*
[22]*August Chełkowski Institute of Physics, University of Silesia, Uniwersytecka 4, 40-007, Katowice, Poland*
[23]*The Henryk Niewodniczański Institute of Nuclear Physics, Polish Academy of Sciences, 152 Radzikowskiego Street, 31-342 Kraków, Poland*
[24]*Dzhelepov Laboratory of Nuclear Problems, Joint Institute for Nuclear Physics, Joliot-Curie 6, 141980 Dubna, Russia*
[25]*Department of Physics, Tomsk State University, 634050 Tomsk, Russia*
[26]*High Energy Accelerator Research Organisation KEK, Tsukuba, Ibaraki 305-0801, Japan*
[27]*Department of Cosmic Ray Physics, National Centre for Nuclear Research, ul. Uniwersytecka 5, 90-950 Łódź, Poland*
[28]*Data Analysis Center at the Institute for Nuclear Studies, Department of Physics, The George Washington University,*
Washington, DC 20052, USA

New data on quasifree polarized neutron-proton scattering in the region of the recently observed *d** resonance
structure are obtained by exclusive and kinematically complete high-statistics measurements with WASA at
COSY. This paper details the determination of the beam polarization, checks of the quasifree character of the
scattering process, on all obtained A_y angular distributions and on the new partial-wave analysis, which includes
the new data producing a resonance pole in $^3D_3$-$^3G_3$ coupled partial waves at $(2380 \pm 10 - i40 \pm 5)$ MeV—in
accordance with the *d** dibaryon resonance hypothesis. The effect of the new partial-wave solution on the

description of total and differential cross-section data as well as specific combinations of spin-correlation and spin-transfer observables available from COSY-ANKE measurements at $T_d = 2.27$ GeV is discussed.

I. INTRODUCTION

Recent measurements of the basic double-pionic fusion to the deuteron, which comprises the reaction channels $pn \to d\pi^0\pi^0$, $pn \to d\pi^+\pi^-$, and $pp \to d\pi^+\pi^0$, reveal a narrow resonance-like structure in the total cross section at a mass $M \approx 2380$ MeV with a width of $\Gamma \approx 70$ MeV [1–3]. From the isospin decomposition of the cross sections in the three fusion channels the isoscalar nature of this structure has been determined [3], whereas the determination of its spin parity $J^P = 3^+$ has been obtained from the angular distributions in the $d\pi^0\pi^0$ channel, which has a particularly low background from conventional reaction processes [2]. Further support for this resonance structure has been found in the $pn \to pp\pi^0\pi^-$ reaction [4], where it was denoted d^* – following its notation associated with the so-called "inevitable" dibaryon [5,6] having identical quantum numbers.

If the observed resonance-like structure constitutes an s-channel resonance in the neutron-proton (np) system, then it has to be sensed also in the observables of elastic np scattering. In Ref. [7] this resonance effect in np scattering has been estimated and it was shown that a noticeable effect should appear in the analyzing power A_y. This observable is most sensitive to small changes in the partial waves, since it is composed only of interference terms between partial waves.

For the analyzing power, there are data only below and above the resonance region. These data sets, at $T_n = 1.095$ GeV ($\sqrt{s} = 2.36$ GeV) [8,9] and $T_n = 1.27$ GeV ($\sqrt{s} = 2.43$ GeV) [10,11], exhibit very similar angular distributions. This gap in the existing measurements of A_y has motivated the present study, the main results of which have been communicated recently in a Letter [12].

II. EXPERIMENT

Measurements of polarized $\vec{n}p$ elastic scattering over the energy region of interest have been carried out in the quasifree mode. The experiment was performed with the WASA detector [13,14] at the COSY storage ring by use of a polarized

deuteron beam of energy of $T_d = 2.27$ GeV, which impinged on the WASA hydrogen pellet target. Utilizing the quasifree scattering process the full energy region of the conjectured resonance was covered. Since we observe here the quasifree scattering process $\vec{d}p \to np + p_{\text{spectator}}$ in inverse kinematics, we were able to detect the fast spectator proton in the forward detector of WASA.

Since elastic np scattering has a large cross section, it was sufficient to have a trigger, which solely required one hit in the first layer of the forward-range hodoscope. Such a hit could originate from either a charged particle or a neutron. In the case of quasifree np scattering we thus have three event classes, with each of them having the spectator proton hit the forward detector:

 (i) Both the scattered proton and the scattered neutron are detected in the central detector. This event type covers the region $31° < \Theta_n^{\text{c.m.}} < 129°$ of neutron angles.
 (ii) The scattered proton is detected in the forward detector, whereas the scattered neutron is not measured. This type concerns the region $132° < \Theta_n^{\text{c.m.}} < 178°$.
 (iii) The scattered proton is detected in the central detector with the neutron being unmeasured, since its scattering angle is outside the angular range of the central detector. This event type covers the angular range $30° < \Theta_n^{\text{c.m.}} < 41°$.

Thus nearly the full range of neutron scattering angles could be covered by the use of all three event classes.

Since, with the use of inverse kinematics, the spectator proton resides in the deuteron beam particle, the emitted spectator proton is very fast, which facilitates its detection in the forward detector. Thus by reconstructing emission angles and kinetic energy the full four-momentum of the spectator proton can be determined.

The four-momentum of the actively scattered proton has been obtained from its track information in either the forward or the central detector. In the latter case the energy information was not retrieved.

In the case where the actively scattered proton has been detected together with its scattering partner, the neutron (case i), we checked, in addition, whether the angular correlation for elastic kinematics was fulfilled. That way we were able to reconstruct the full event, which includes also the four-momentum of the neutron. In the case where the neutron was not measured, the subsequent kinematic fit had one overconstraint in case ii and none in case iii. In the case where the neutron could be detected by a hit in the calorimeter [composed of 1012 CsI(Na) crystals] of the central detector—associated with no hit in the preceding plastic scintillator barrel—the directional information on the scattered neutron could be retrieved. Therefore, such events, which correspond to case i, have undergone a kinematic fit with two overconstraints.

———————

*clement@pit.physik.uni-tuebingen.de

†Present address: Albert Einstein Center for Fundamental Physics, University of Bern, Sidlerstrasse 5, 3012 Bern, Switzerland.

‡Present address: Department of Physics and Astrophysics, University of Delhi, Delhi-110007, India.

§Present address: Institut für Kernphysik, Johannes Gutenberg-Universität Mainz, Johann-Joachim-Becher Weg 45, 55128 Mainz, Germany.

‖Present address: Department of Physics and Astronomy, University of Sheffield, Hounsfield Road, Sheffield S3 7RH, United Kingdom.

A. Determination of the beam polarization

In order not to distort the beam polarization, the magnetic field of the solenoid in the central detector was switched off. The measurements were carried out with cycles of the beam polarization "up," "down," and "unpolarized" (originating from the same polarized source), where up and down refer to a horizontal scattering plane. Runs with the conventional unpolarized source verified that the beam originating from the polarized source indeed was unpolarized when it was used in its unpolarized mode.

The magnitude of the beam polarization has been determined and monitored by dp elastic scattering, which was measured in parallel by detecting the scattered deuteron in the forward detector as well as the associated scattered proton in the central detector. In the case of a transversally polarized deuteron beam the dependence of the count rate $N(\Theta,\Phi)$ on the polar and azimuthal scattering angles Θ and Φ is given by

$$N(\Theta,\Phi) \sim 1 + \tfrac{3}{2}P_z A_y(\Theta)\cos\Phi + \tfrac{1}{4}P_{zz}[A_{xx}(\Theta)(1-\cos 2\Phi)$$
$$+ A_{yy}(\Theta)(1+\cos 2\Phi)]. \tag{1}$$

Here P_z and P_{zz} denote vector and tensor polarization of the deuteron beam, whereas A_y, A_{xx}, and A_{yy} are the respective vector and tensor analyzing powers of the dp scattering process.

With WASA covering the full azimuthal angular range, we may decompose vector and tensor parts by fitting the observed azimuthal angular dependence for specific polar angles by use of Eq. (1). The absolute values for the vector and tensor components of the deuteron beam have been obtained by fitting our results for the vector A_y [Fig. 1(a)] and tensor analyzing power A_{yy} [Fig. 1(b)] in absolute height to those obtained previously at ANL [15] for $T_d = 2.0$ GeV. Though this energy is somewhat below the one used here, the analyzing powers in pd scattering have been observed [15,16] to be only weakly dependent on the beam energy. This is supported by very recent data obtained at COSY-ANKE [17] at $T_d = 2.27$ GeV. As a result we obtain beam polarizations of $P_z = 0.67(2)$, $P_{zz} = 0.65(2)$ for up and $P_z = -0.45(2)$, $P_{zz} = 0.17(2)$ for down. For the determination of P_{zz} we concentrated on the most forward angles, where the ANL and COSY-ANKE results agree with each other. In addition, the cross section is largest there, thus minimizing background contaminations.

B. Checks of quasifree scattering

The vector polarization of the beam for quasifree scattering has been checked by quasifree pp scattering, which also was measured in parallel by detecting one of the protons in the forward detector and the other one in the central detector— and, in addition, checking their angular correlation for elastic kinematics. If the proton in the beam deuteron is at rest, then its momentum corresponds to just half of the beam momentum. Note that in the energy region of interest here, the pp analyzing power does not exhibit any significant energy dependence, hence we do not need to correct for the energy smearing due to the Fermi motion of the proton. Figure 2 shows our results from the quasifree pp scattering for the analyzing power. Figure 2(a)
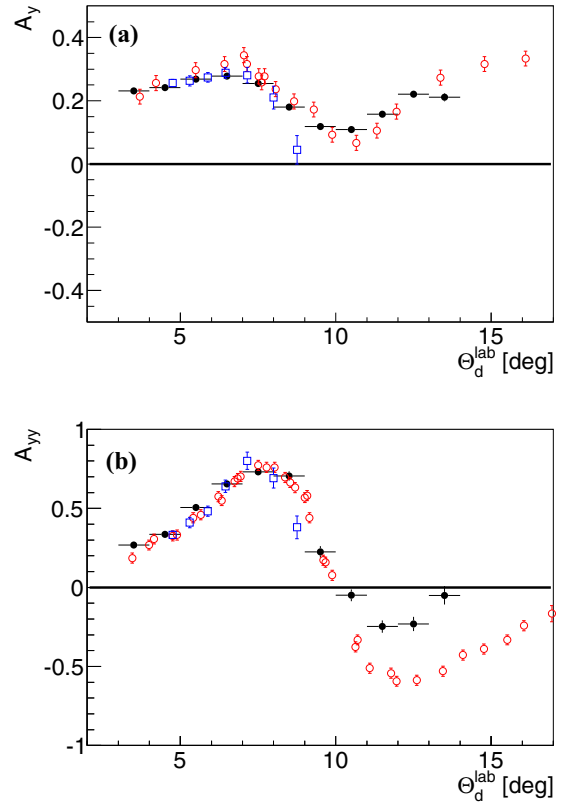

FIG. 1. (Color online) Angular distributions of vector [A_y; (a)] and tensor [A_{yy}; (b)] analyzing powers in dp scattering at $T_d = 2.27$ GeV. Filled circles denote results from this work averaged over beam polarization "up" and "down" runs, whereas open symbols denote results previously obtained at Argonne National Laboratory at $T_d = 2.0$ GeV [15] (open circles) and COSY-ANKE at $T_d = 2.27$ GeV [17] (open squares). Error bars denote statistical uncertainties.

shows the angular distribution in comparison with the EDDA measurements [18] of free pp scattering. The solid curve gives the SAID phase-shift solution SP07 [19], which, again, is based in this energy range on the EDDA data.

In order to check whether the proton polarization depends on the effective energy of the quasifree incident protons, we reconstruct the effective center-of-mass energy $\sqrt{s}$ for each event. In this way we obtain angular distributions sorted into six $\sqrt{s}$ bins, which we compare to the SAID SP07 phase-shift predictions for these energies. The ratio of our pp data to the SAID prediction at each of these energies is plotted in Fig. 2(b). Though the figure might indicate a very slight trend toward energy dependence, within uncertainties the proton polarization can be considered to be constant within 1% over the energy interval covered by this experiment.

The momentum distribution of the observed spectator proton in the elastic np scattering process is plotted in Fig. 3 in the deuteron rest frame, where it is compared with Monte Carlo simulations of the proton momentum distribution in a deuteron filtered by the acceptance of the WASA detector. In these simulations the CD Bonn potential [20] deuteron wave
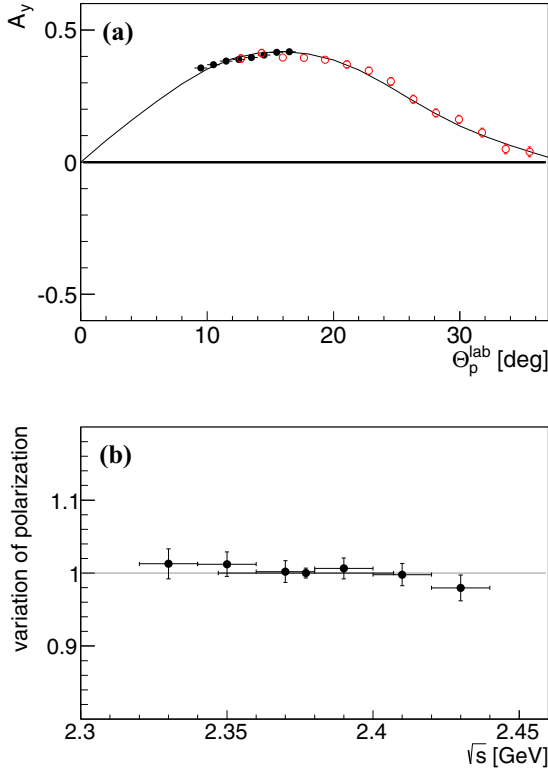
FIG. 2. (Color online) (a) Vector analyzing power A_y in pp scattering at $T_p = 1.135$ GeV. Filled circles denote results from this work, whereas open symbols denote results previously obtained with EDDA at $T_p = 1.132$ GeV [18]. The solid line represents the SAID SP07 phase-shift solution [19]. (b) Variation of the proton polarization over the measured energy interval plotted as the ratio to the SAID SP07 phase-shift solution. The datum at 2.377 GeV derives from (a) and denotes the average over the full energy range covered in this experiment.

function has been used. Due to the beam pipe, ejectiles can only be detected in the forward detector for laboratory angles larger than $3°$. In order to assure a quasifree process we omit events with spectator momenta larger than 0.16 GeV/c (in the deuteron rest system) from the subsequent analysis—as done in previous work [2–4].

III. RESULTS AND DISCUSSION

A. A_y angular distributions

Since we have measurements with spin "up," with spin "down," and unpolarized, the vector analyzing power for np scattering can be derived in three ways, by using each two of the three spin situations. All three methods should give the same results. Differences in the results may be taken as a measure of systematic uncertainties, which are added quadratically to the statistical ones to give the total uncertainties.

In Fig. 4 we show the results for A_y, if we combine measurements either with spin up and unpolarized (open circles) or with spin down and unpolarized (filled squares) for extracting A_y. The values for the combination up and down are just in between (filled circles). For this plot the data are used without accounting for the spectator momentum, i.e., without
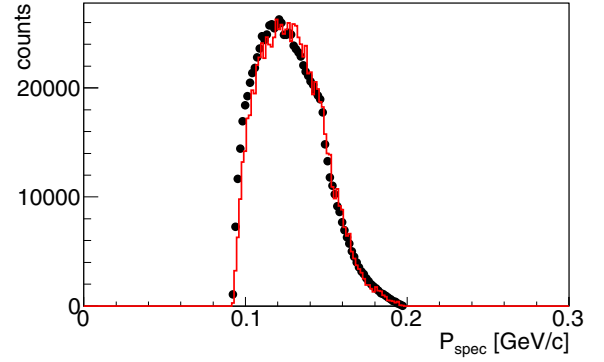

FIG. 3. (Color online) Distribution of spectator proton momenta (in the deuteron rest frame) in the $dp \rightarrow pn + p_{spectator}$ reaction within the acceptance of the WASA detector. Data are given by filled circles. The solid line shows the expected distribution for the quasifree process based on the CD Bonn potential [20] deuteron wave function. For data analysis, only events with $p_{spectator} < 0.16$ GeV/c were used.
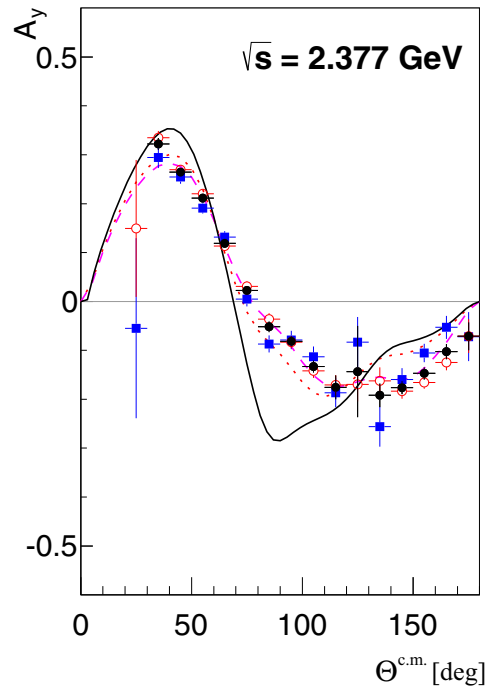

FIG. 4. (Color online) Angular distributions of the np analyzing power without consideration of the spectator momentum, i.e., without classifying the collected pn scattering events according to their effective total center-of-mass energy $\sqrt{s}$. That way the data set corresponds to the weighted average over the measured interval representing effectively the range $\sqrt{s} = 2.377 \pm 0.03$ GeV (corresponding to 1.075 GeV $\leqslant T_n \leqslant$ 1.195 GeV). Open circles and filled squares denote A_y extraction by the combination "up" with "unpolarized" and "down" with "unpolarized," respectively. Filled circles give the statistically weighted average over both methods. Error bars denote statistical uncertainties. The solid line represents the SAID SP07 phase-shift solution [19], whereas the dashed (dotted) line gives the result of the new weighted (unweighted) SAID partial-wave solution (see text).
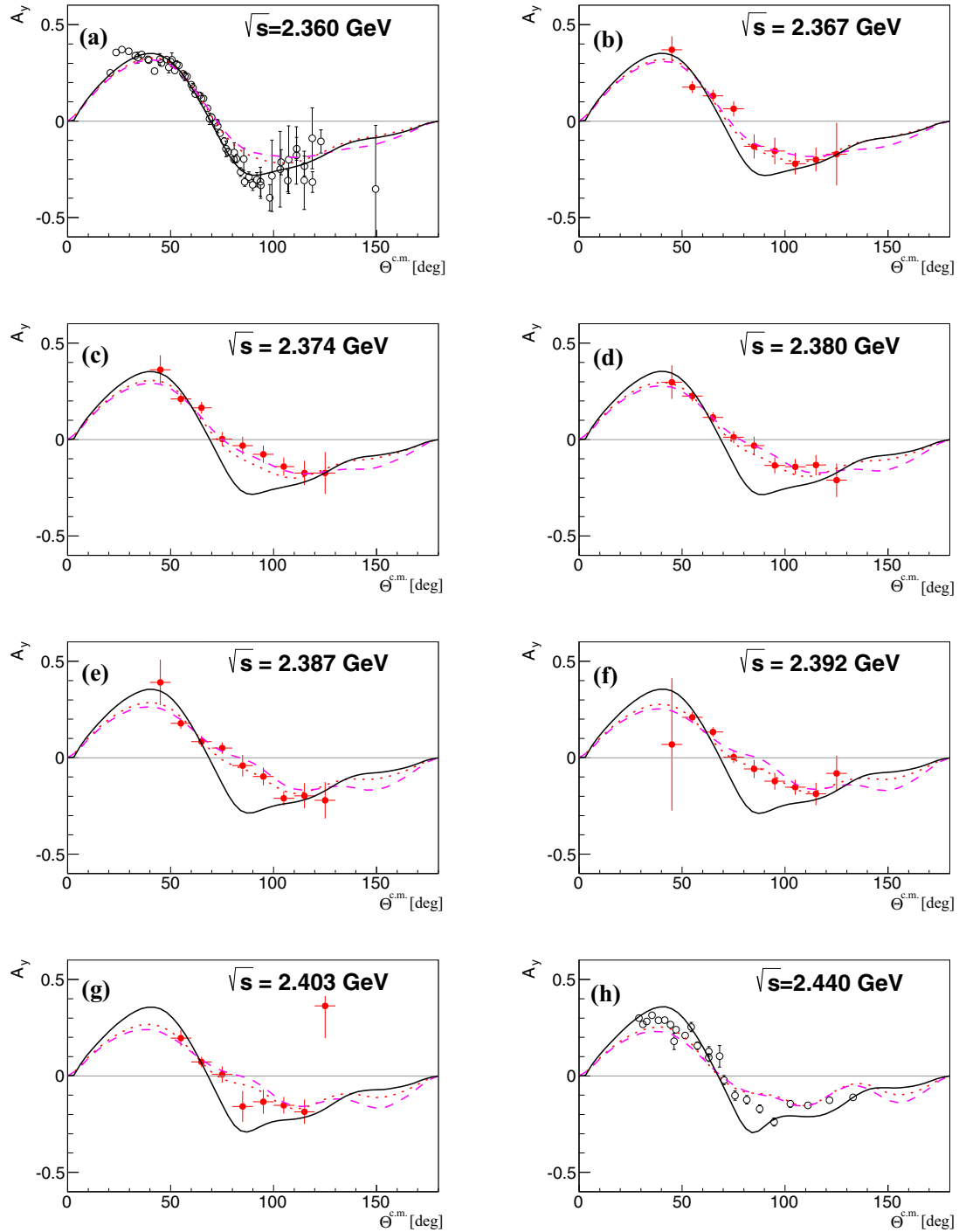
FIG. 5. (Color online) A_y angular distributions for $\sqrt{s}$ = 2.360, 2.367, 2.374, 2.380, 2.387, 2.392, 2.403, and 2.440 GeV, corresponding to T_n = 1.095, 1.108, 1.125, 1.139, 1.156, 1.171, 1.197, and 1.27 GeV. Filled symbols denote results from this work taking into account the spectator four-momentum information. Error bars on filled symbols include both statistical and systematic uncertainties. Open symbols denote previous work [8–11]. Solid lines represent the SAID SP07 phase-shift solution [19], whereas dashed (dotted) lines give the result of the new weighted (unweighted) SAID partial-wave solution (see text).

selection according to the np center-of-mass energy. Thus this data set corresponds to the weighted average over the covered interval of $\sqrt{s}$.

Due to the Fermi motion of the nucleons bound in the beam deuteron, the measurement of the quasifree np scattering process covers a range of energies in the np system. Meaningful

statistics could be collected for the range of np center-of-mass energies $2.37 < \sqrt{s} < 2.40$ GeV corresponding to $T_n = 1.11$–1.20 GeV.

By taking into account the measured spectator four-momentum we may construct the effective $\sqrt{s}$ for each event. In this way we obtain angular distributions sorted in
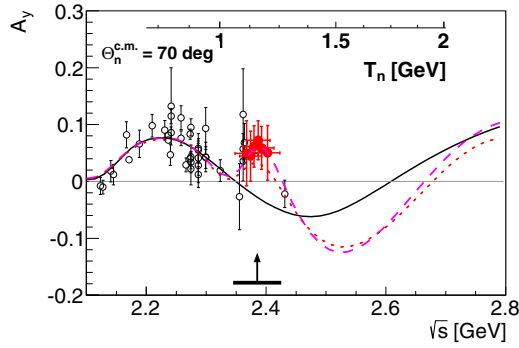
FIG. 6. (Color online) Energy dependence of the *np* analyzing power at $\Theta_n^{\text{c.m.}} = 70°$. Filled symbols denote the results of this work; open symbols, those from previous work [8–10,22–27]. For the meaning of the curves see Fig. 4. The vertical arrow and horizontal bar indicate the pole and width of the resonance.

$\sqrt{s}$ bins. In order to have sufficient count-rate statistics we restricted this procedure to data sets in the angular region $31° < \Theta_n^{\text{c.m.}} < 129°$ and divided the available energy range into six bins, which are shown in Fig. 5 together with the SAID SP07 solution (solid lines) and the new solution (see next section), which contains a resonance pole (dashed and dotted lines). We also include in Fig. 5 previously obtained angular distributions at $\sqrt{s} = 2.360$ and 2.440 GeV ($T_n = 1.095$ and 1.27 GeV) [8–11], which are closest to the resonance region covered here. Note that these angular distributions, being below and above the resonance region, exhibit a significantly different angular behavior—in particular, at medium angles.

In Fig. 6 we show as an example the energy dependence of A_y at $\Theta_n^{\text{c.m.}} = 70°$ (see also Fig. 4 in Ref. [12]), where the energy dependence at $\Theta_n^{\text{c.m.}} = 83°$ is depicted. The trend of the new data in the resonance region deviates clearly from that exhibited by the data from previous experiments below and above this region [8–10,22–27]. The new partial-wave solutions (see below) connect all data within their uncertainties, whereas the SP07 solution obviously fails in the resonance region.

The decomposition of the *np* scattering observables into partial-wave amplitudes is given in Ref. [21]. Accordingly we have, for the analyzing power,

$$d\sigma/d\Omega * A_y \sim \text{Im}(H_3 + H_5)H_4^*, \qquad (2)$$

with H_i containing sums over partial-wave amplitudes with total angular momenta $j_0 = j = L$, $j_- = L - 1$, and $j_+ = L + 1$. H_3 contains terms proportional either to the Legendre polynomials P_j or to the associated ones P_j^1. In H_5 there are terms only proportional to P_j, and in H_4, terms only proportional to P_j^1. In particular, the structure of H_4 for $j = 3$ is as follows:

$$H_4(j = 3) \sim [4(T_{L=4} - 3T_{L=2}) + \sqrt{12}T_{L=3}]P_3^1, \qquad (3)$$

where the *T*-matrix elements contain the complex phase shifts. We see that a resonance effect in $^3D_3$ and $^3G_3$ enters with opposite sign and is proportional to P_3^1 in both cases. Hence the resonance effect vanishes at the zeros of P_3^1, which is the case at $\Theta = 63.4°$ and $116.6°$. At these angles the predictions

with and without resonance in $^3D_3$ or $^3G_3$ should cross each other. If, in the SP07 solution and in the new solution, the nonresonant contributions are essentially the same, then the angular distributions calculated with these solutions should cross at these angles. Figure 5 demonstrates that this is the case in good approximation. Upon observing the maximum deviations from the SP07 solution in the angular region around $90°$ as well as the minimum deviations around $63°$ and $117°$—coupled with a sign change thereafter—one can see that both the data and the new SAID solutions exhibit the characteristic features of the P_3^1 function and thus uniquely point to the signature of a $J^P = 3^+$ resonance in the elastic *np* scattering.

The horizontal bars on the data points in Fig. 6 (and also in Fig. 4 in Ref. [12]) include both the range of the $\sqrt{s}$ bins and the uncertainties in the determination of the $\sqrt{s}$ values reconstructed for each event. Since we deal here with only zero to two overconstraints in the kinematic fits, the $\sqrt{s}$ determination is less precise than, e.g., in the $pd \to d\pi^0\pi^0 + p_{\text{spectator}}$ reaction, where we have three overconstraints in the case where the proton spectator is not detected.

B. Partial-wave analysis

The new A_y data have been included in the SAID database and the phenomenological approach used in generating the *NN* partial-wave solution, SP07 [19], has been retained. Here we simply consider whether the existing form is capable of describing the new A_y measurements. One advantage of this approach is that the employed Chew-Mandelstam *K* matrix can produce a pole in the complex energy plane without the explicit inclusion of a *K*-matrix pole in the fit form. Neither the existence of a pole nor the effected partial waves are predetermined.

The energy-dependent fits use a product *S*-matrix approach as described in detail in Ref. [28], with S_x being an "exchange" part, including the one-pion-exchange piece plus smooth phenomenological terms, and S_p a "production" part. The full *S* matrix is

$$S = S_x^{1/2} S_p S_x^{1/2} = 1 + 2iT, \qquad (4)$$

where

$$T = T_x + S_x^{1/2} T_p S_x^{1/2}. \qquad (5)$$

For spin-uncoupled waves, the production *T* matrix is parameterized using a Chew-Mandelstam *K* matrix, as is also used in the GW πN [29] and KN [30] analyses, with

$$T_p = \rho^{1/2}K_p(1 - CK_p)^{-1}\rho^{1/2}, \qquad (6)$$

where ρ is a phase-space factor, K_p is a real symmetric matrix coupling the *NN* and an inelastic channel, and *C* is a Chew-Mandelstam matrix. For isovector waves, the inelastic channel is identified as $N\Delta$; in the isoscalar case, this inelastic channel is generic. For spin-uncoupled waves, the matrices are 2×2; for coupled waves, the matrices are 3×3, as described in Ref. [28]. The global energy-dependent fit includes *pp* data from threshold up to a laboratory kinetic energy of 3 GeV, and *np* data from threshold up to 2 GeV. Since above

1.3 GeV the np data are sparse, the fit is considered to be valid only up to 1.3 GeV for the np case. Single-energy (narrow-energy-bin) fits are also carried out with constraints on the energy dependence over a particular energy bin fixed to the underlying global analysis.

The new A_y data are angular distributions at T_{Lab} values of 1.108, 1.125, 1.135, 1.139, 1.156, 1.171, and 1.197 GeV. Starting from the functional form of the current SP07 fit, and varying only the associated free parameters, a χ^2/datum of 1.8 was found for all angular distributions apart from the one at 1.135 GeV. This is fairly consistent with the overall χ^2/datum given by the global fit of np to 2 GeV. However, the set at 1.135 GeV contributes a χ^2/datum of about 25 and has better statistics and a wider angular coverage.

The fit form was scanned to find partial waves for which an added term in the K-matrix expansion produced the most efficient reduction in χ^2. Adding parameters and refitting resulted in a rapid variation of the coupled $^3D_3$ and $^3G_3$ waves in the vicinity of the problematic 1.135-GeV data set.

Some weighting seemed necessary in this fit, as only a few angular points from the full set were determining the altered energy dependence. The fit was repeated with different weightings (with a factor of 2 or 4) for the new A_y data. Initially, the full set of energies was weighted equally. However, it was found that just weighting the 1.135-GeV angular distribution improved the fit to the new analyzing power data at all energies. The results reported here thus consider only the weighting at this single energy. As we have seen in fits to other reactions, heavily weighting new and precise polarization observables inevitably degrades the fit to older data. Therefore, as a test, the parametrization producing a pole was refitted to the full database with no weighting. This gave, as expected, a worse fit to the 1.135-GeV angular distribution but did not change the shape qualitatively.

In Figs. 4–6 and 9–11 we plot the SP07 prediction (not including the new data), a weighted fit (errors decreased by a factor of 4), and an unweighted fit including the new data and using the fit form having added parameters. Resulting changes in the $^3D_3$-$^3G_3$ coupled waves are displayed in Fig. 3 in Ref. [12]. Note that the single-energy solutions obtained previously for energies up 1.1 GeV fit better to the new partial-wave solution than to SP07.

In the new solution the $^3D_3$ wave obtained a typical resonance shape, whereas the $^3G_3$ wave changed less dramatically. In Fig. 7 the Argand diagrams of the new partial-wave solution are shown for $^3D_3$ and $^3G_3$ partial waves as well as for their mixing amplitude ϵ_3. In the Argand diagram the $^3D_3$ partial wave exhibits an abrupt change at the pion production threshold ($\sqrt{s} = 2.02$ GeV), when absorption sets in, followed by a pronounced looping in the d^* energy region, before it enters the region of the conventional t-channel $\Delta\Delta$ process [1–4] at the highest energies. In the Argand diagrams of $^3G_3$ and ϵ_3 also a looping is observed in the d^* region, though much less pronounced.

A search of the complex energy plane revealed a pole in the coupled $^3D_3$-$^3G_3$ wave. Other partial waves did not change significantly over the energy range spanned by the new data.
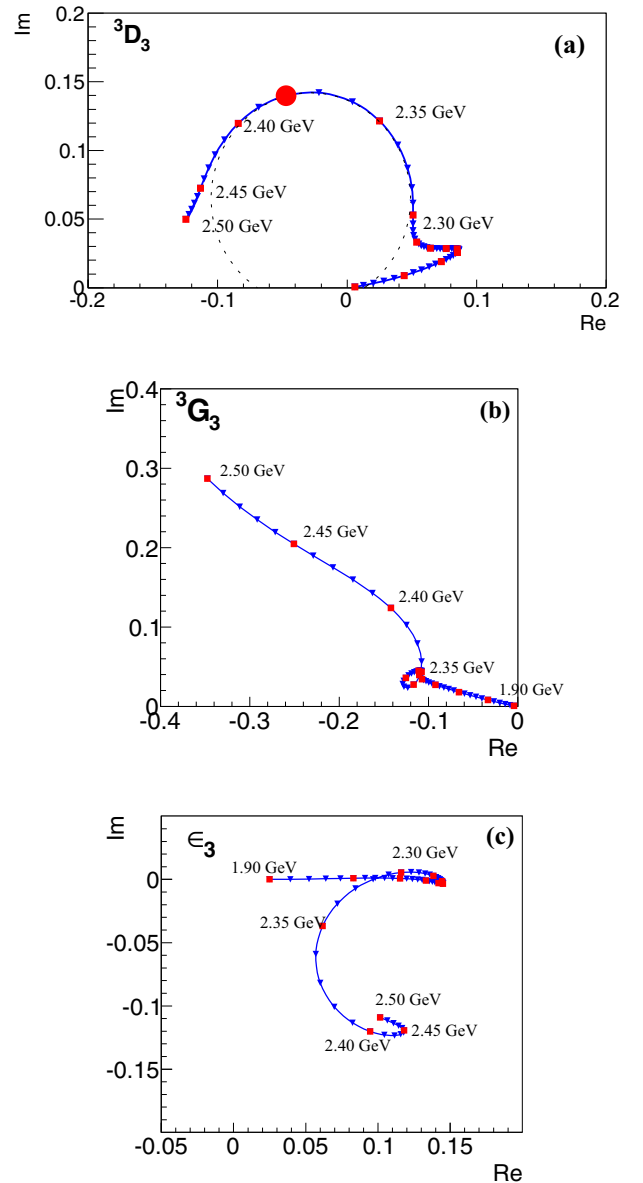

FIG. 7. (Color online) Argand diagrams of $^3D_3$ (a) and $^3G_3$ (b) partial waves as well as of their coupling amplitude ϵ_3 (c) in the new partial-wave solution. Values are plotted as small filled triangles in 10-MeV steps and as small squares in 50-MeV steps, together with the corresponding total energy $\sqrt{s}$. The thick filled circle gives the energy position of the resonance pole. The dotted curve in (a) is a circle fitted to the loop; its diameter equals the branching ratio B_{el}.

The fit repeated with different weightings for the new A_y data resulted in a variation of the pole position and could be considered a minimal "error" on its value within the present fit form. In the weighted fits, a pole was located at (2392–i37) MeV. The refit without weighting produced a pole with (2385–i39) MeV.

For the $^3D_3$ partial wave we display in Fig. 8 a speed plot as defined in Refs. [31,32]. It exhibits a Lorentz-like shape with a maximum at 2.37 GeV and a width of about 80 MeV. Hence together with the speed-plot determination we arrive at
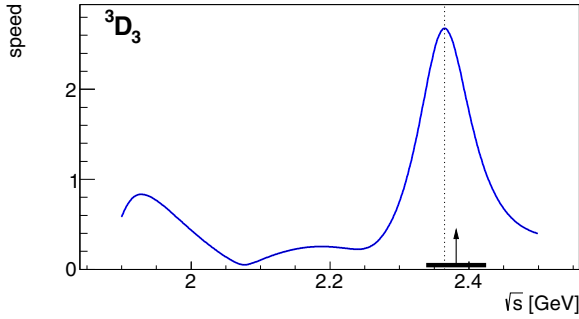
FIG. 8. (Color online) Speed plot of the $^3D_3$ partial wave. The dotted vertical line indicates the position of the maximum. The vertical arrow and horizontal bar indicate the pole and width of the resonance as averaged over the values obtained in contour and speed plots (see text).

$(2380 \pm 10 - i40 \pm 5)$ MeV as our best estimate for the pole position.

As pointed out by Höhler [31], both Argand diagram and speed plot also allow the determination of the modulus r of the residue, which corresponds to just half of the partial decay width Γ_{el} of the resonance into the elastic channel. Since according to Höhler the radius of the resonance circle in the Argand diagram equals just half the branching ratio $B_{el} = \Gamma_{el}/\Gamma$, we derive, from the Argand diagram plotted in Fig. 7(a), a value of $B_{el} = 0.15$. The height H of the Lorentz-like peak above background in the speed plot is related to the branching ratio by $H = 2B_{el}/\Gamma$, which leads to $B_{el} = 0.10$. These numbers depend somewhat, of course, on the assumption of the background. Hence, as our best estimate for the branching ratio we take the average $B_{el} = 0.12 \pm 0.03$ (corresponding to $r = 5 \pm 1$ MeV). This value agrees very well with the expectation based on unitarity and the knowledge about the various two-pion decay channels of the intermediate $\Delta\Delta$ system, which d^* decays into [7].

In addition to the modulus r of the residue, its phase ϕ can also be determined—most favorably from the Argand diagram of the derivative of the partial-wave amplitude [31,32]— though usually with a much lower accuracy. Here, we obtain values for ϕ between $-21°$ and $+9°$, depending on the details of the procedure.

IV. COMPARISON OF THE NEW PARTIAL-WAVE SOLUTION TO FURTHER OBSERVABLES OF NEUTRON-PROTON SCATTERING

In the following we compare the new SAID partial-wave solution to all data related to the np scattering issue, which are available for the energy region of interest.

A. Total cross section

In Ref. [7] the contribution of the d^* resonance to the total np cross section has been estimated to be around 1.5 mb. Though this is small compared to the total cross section of 38 mb in the resonance region, it is larger than the uncertainties quoted in the total cross-section measurements by Devlin *et al.* [34]. In fact, the total np cross-section data exhibit a significant
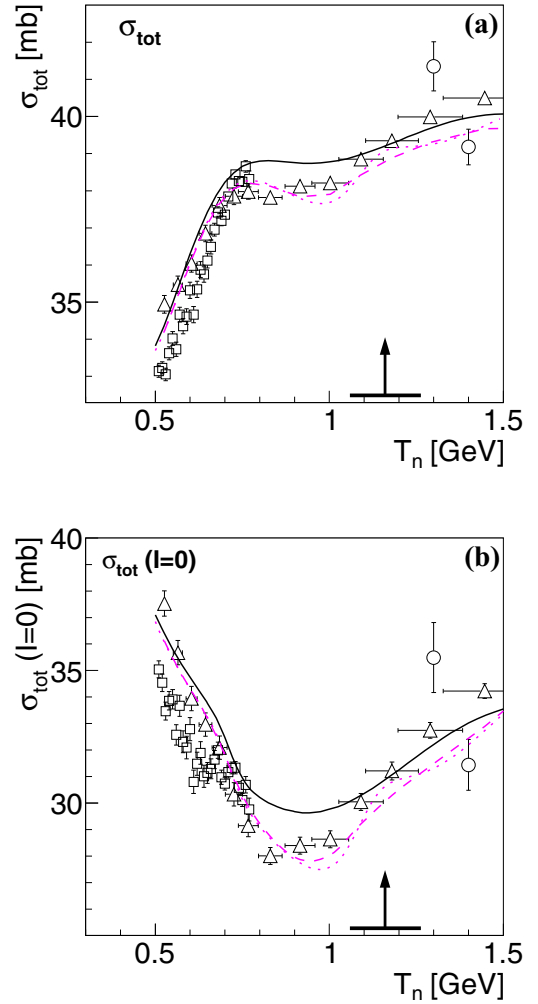

FIG. 9. (Color online) Total *pn* cross-section (a) and total isoscalar nucleon-nucleon cross-section (b) dependence of the incident neutron (nucleon) energy T_n. Data are from Lisowski *et al.* [33] (open squares), Devlin *et al.* [34] (open triangles), and Sharov *et al.* [35] (open circles). Horizontal bars indicate the energy resolution of the incident neutrons. Solid and dashed curves, representing the SP07 and the new solution, respectively, are averaged over the experimental energy resolution of Ref. [34]. The dotted line gives the new solution without averaging over the experimental energy resolution. The vertical arrow and horizontal bar indicate the pole and width of the resonance.

rise in this region, whereas the total pp cross section is flat in the region of interest.

Fig. 9(a) shows the total np cross section for $T_n = 0.5$–1.5 GeV. The data plotted with open squares for $T_n < 0.8$ GeV are from Lisowski *et al.* [33], taken at LAMPF in a high-resolution dibaryon search. The other data, plotted with open triangles, are from Devlin *et al.* [34], taken with a neutron energy resolution of 4%–20% (horizontal bars in Fig. 5). Also, data from Sharov *et al.* [35] are shown (open circles), which have larger uncertainties but are taken with the much superior neutron energy resolution of 13–15 MeV. The data exhibit a pronounced jump in the cross section between $T_n = 1.0$ GeV and $T_n = 1.3$ GeV. This jump is remarkable,
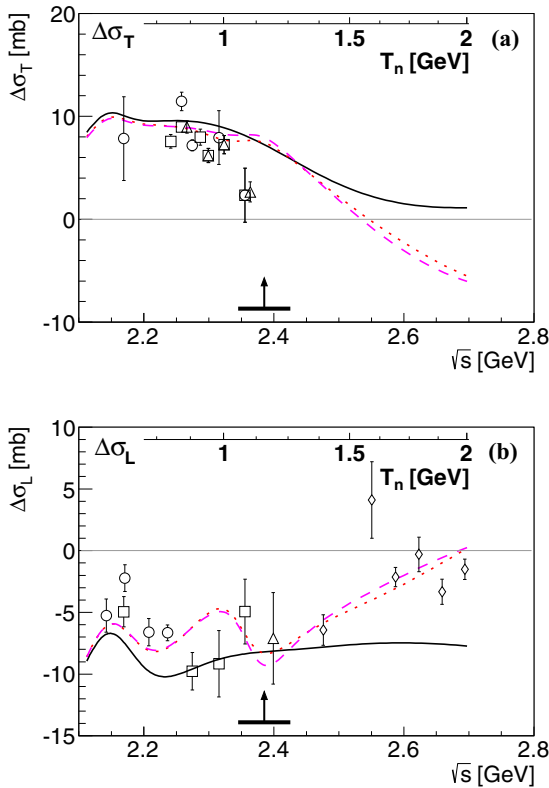
FIG. 10. (Color online) Energy dependence of the transversal (a) and longitudinal (b) total np cross-section differences. Symbols denote data from Refs. [9,35–40]. For the meaning of the curves see Fig. 4. The vertical arrow and horizontal bar indicate the pole and width of the resonance.
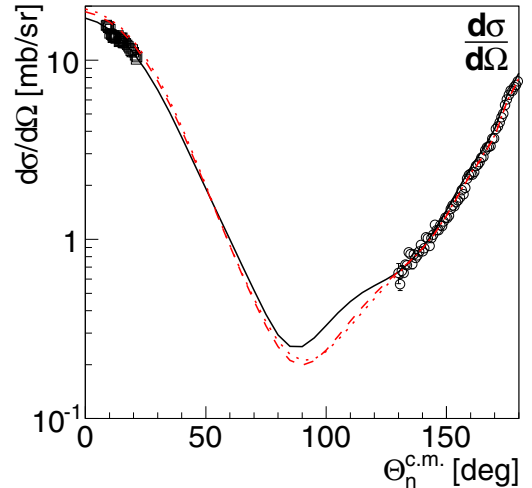

FIG. 11. (Color online) Angular distribution of the differential cross section $d\sigma/d\Omega$ at $T_n = 1.135$ GeV corresponding to the resonance energy $\sqrt{s} = 2.38$ GeV. For the meaning of the curves see the caption to Fig. 4. Plotted data are from Ref. [41] ($T_n = 1.135$ GeV) and Ref. [42] ($T_n = 1.118$ GeV).

for $\Delta\sigma_T$, they deviate substantially from each other for $\Delta\sigma_L$. On average, the new solution gives a superior description of the $\Delta\sigma_L$ data, in particular, in and above the resonance region.

B. Differential cross section

Figure 11 shows the angular distribution of the differential cross section $d\sigma/d\Omega$ for elastic np scattering at $T_n = 1.135$ GeV corresponding to the resonance energy $\sqrt{s} = 2.38$ GeV, where we expect the effect of the resonance on the observables to be largest. At this energy there are only data for the differential cross section at very forward and backward scattering angles. The solid line denotes the current SAID SP07 solution, and the dashed (dotted) line gives the result with the new weighted (unweighted) SAID solution. The resonance effect is small though noticeable in the differential cross section, since, in contrast to the analyzing power, the partial-wave amplitudes enter only quadratically. The resonance effect is predicted to be most notable at intermediate angles, where the differential cross section gets smallest and where, as of yet, no data are available.

C. Spin-correlation and spin-transfer observables

As of yet there are no direct measurements of spin-correlation and spin-transfer measurements in the resonance region. However, at COSY-ANKE the reaction $\vec{d}\vec{p} \rightarrow n[pp]_s$ has been measured at various energies [43], where $[pp]_s$ indicates that the proton pair is in a relative $^1S_0$ state. At ANKE this has been achieved experimentally by requiring the relative kinetic energy of the two protons to be lower than 3 MeV.

This reaction is correlated with np scattering in the impulse approximation. Whereas the obtained polarization observables agree very well with calculations based on the SAID SP07 solution for $T_d < 2$ GeV, these measurements show large deviations at $T_d = 2.27$, which corresponds just

since the pp total cross section is completely flat in this energy region. Hence in the isoscalar total nucleon-nucleon cross section $\sigma_{I=0} = 2\sigma_{pn} - \sigma_{pp}$, where the SAID values are used for σ_{pp}, this effect appears still more pronounced [Fig. 9(b)]. The current SAID SP07 solution is shown by the solid lines again. Its description of the data is only fair. In particular, the observed increase in the total cross section above 1 GeV is only slightly indicated in the SAID SP07 solution. The dotted lines show the new weighted partial-wave solution, which includes the resonance pole. They exhibit a clear s-shaped resonance behavior. The dashed lines are averaged over the experimental resolution of the data of Devlin *et al.* [34] and provide a preferable description of the data.

In Fig. 10 we show the total np cross sections measured in dependence of the spin directions of the beam and target particles. These spin-dependent total cross sections are measured with the directions of the beam and target polarizations being either parallel or antiparallel. For the so-called transversal total cross-section difference $\Delta\sigma_T$ the polarization vectors are transversally oriented with respect to the beam direction. For the so-called longitudinal cross-section difference $\Delta\sigma_L$ they are longitudinally oriented.

For $\Delta\sigma_T$ measurements exist only for energies below the resonance region, but for $\Delta\sigma_L$, measurements extend to energies well above this region. Whereas the SP07 and new solutions nearly coincide below and in the resonance region

TABLE I. Deuteron-proton tensor analyzing powers and spin-correlation parameters at $T_d = 2.27$ GeV and $q = 0$ obtained from SAID SP07 [19] and new partial-wave solutions by use of Eqs. (7) and (8) in comparison with experimental results from COSY-ANKE [43].

Observable	Experiment	SP07	New solution
$A_{xx}(0) = A_{yy}(0)$	$-0.38(3)$	-0.30	-0.42
$C_{x,x}(0) = C_{y,y}(0)$	$-0.39(5)$	-0.48	-0.31

to the resonance energy. A simple relation of the ANKE polarization observables to specific ones of np scattering is obtained in the pp $^1S_0$ limit at $\Theta_n^{\text{c.m.}} = 180°$ [44,45] for the deuteron-proton tensor analyzing powers

$$A_{xx}(q = 0) = A_{yy}(q = 0)$$
$$= 2\frac{K_{0ll0}(\pi) - K_{0nn0}(\pi)}{3 - K_{0ll0}(\pi) - 2K_{0nn0}(\pi)} \qquad (7)$$

and spin-correlation parameters

$$C_{x,x}(q = 0) = C_{y,y}(q = 0)$$
$$= 2\frac{A_{00nn}(\pi) - D_{n0n0}(\pi)}{3 - K_{0ll0}(\pi) - 2K_{0nn0}(\pi)}, \qquad (8)$$

where q is the momentum transfer between initial neutron and final proton. Here A_{ijkl}, D_{ijkl}, and K_{ijkl} denote np spin-correlation and spin-transfer parameters.

ANKE finds $A_{xx} = -0.38(3)$ and $C_{x,x} = -0.39(5)$ at $T_d = 2.27$ GeV (Table I). Calculating these observables with the SP07 solution results in values of -0.30 and -0.48, respectively, which are significantly different. However, the new SAID solution gives $A_{xx} = -0.42$ and $C_{x,x} = -0.31$, which are closer to the ANKE experimental values.

V. SUMMARY AND CONCLUSIONS

The exclusive and kinematically complete measurements of quasifree polarized np scattering with WASA at COSY have provided detailed high-statistics data for the analyzing power in the energy range, where a narrow resonance structure with $I(J^P) = 0(3^+)$, called d^*, was observed previously in double-pionic fusion to the deuteron. A partial-wave analysis including these new data exhibits a resonance pole at $(2380 \pm 10 - i40 \pm 5)$ MeV in $^3D_3$-$^3G_3$ coupled partial waves—thus establishing the $d^*(2380)$ resonance structure to be a genuine s-channel resonance. This constitutes the first clear-cut experimental finding of a true dibaryon resonance.

This resonance was first observed in the $pn \to d\pi^0\pi^0$ reaction. The Dalitz plot in Ref. [2] shows that the resonance predominantly decays via an intermediate $\Delta\Delta$ configuration. Exactly such a state with identical quantum numbers was predicted first by Dyson and Xuong [46] based on SU(6) symmetry breaking in 1964—just shortly after Gell-Mann's publication of the quark model [47]. Whereas this dibaryon state was denoted D_{03} in Ref. [46], it was later named d^* by Goldman *et al.* [5], who pointed out the unique symmetry properties of such a state with these quantum numbers, calling it the "inevitable" dibaryon.

So $d^*(2380)$ may be associated with a bound $\Delta\Delta$ resonance, which could contain a mixture of asymptotic $\Delta\Delta$ and six-quark, hidden-color configurations [48]. Recent quark-model calculations [49–51] find this state at a mass close to the experimental one. Whereas the width calculated in Ref. [49] is still substantially too large, the one obtained in Ref. [51] is already in good agreement with the experimental finding, as soon as coupling to hidden-color configurations is accounted for. New three-body calculations [52,53] of the Faddeev type with relativistic kinematics and hadron dynamics find $d^*(2380)$ at the right mass and an only slightly larger width.[1]

In addition to np scattering, evidence for d^* has been found so far in the two-pion production reactions $pn \to d\pi^0\pi^0$, $pn \to d\pi^+\pi^-$, and $pn \to pp\pi^0\pi^-$. So the only remaining hadronic channels where d^* should contribute are $np\pi^0\pi^0$ and $np\pi^+\pi^-$. The first one has been studied at WASA and the results will be published [54]. The latter channel has been measured at HADES and preliminary results have been reported at conferences. This means that all major channels of d^* decay will have been investigated in the near-future. All decay branches into the two-pion decay channels appear to be well accounted for by isospin relations [7].

It is amazing that the simple but basic estimate by Dyson and Xuong [46] in 1964 is very close to the now observed mass of d^* alias D_{03}. Together with the results of the new calculations based on quark [49–51] and/or hadron [52,53] dynamics, this might instill some confidence in the predictive power of these theoretical considerations for further dibaryon states.

We, finally, note that very recently an alternative explanation of the WASA data was suggested by D. V. Bugg [55]. Among the issues raised in this paper, we mention just one here. The specific intermediate $NN^*(1440)$ system proposed for the production of the narrow resonance-like structure is not restricted to the isoscalar channel and hence should show up both in np- and in pp-initiated two-pion production. However, as we have shown, this narrow resonance structure is missing in all pp-initiated two-pion production channels including double-pionic fusion [3,56–59].

———

[1]In Refs. [52,53] a width suppression factor has been introduced, which is at variance with our observations for $d^* \to pp\pi^0\pi^-$ decay [4]. Hence only the values for the width without this factor should be compared to the experimental one.

[1] M. Bashkanov *et al.*, Phys. Rev. Lett. **102**, 052301 (2009).
[2] P. Adlarson *et al.*, Phys. Rev. Lett. **106**, 242302 (2011).
[3] P. Adlarson *et al.*, Phys. Lett. B **721**, 229 (2013).
[4] P. Adlarson *et al.*, Phys. Rev. C **88**, 055208 (2013).
[5] T. Goldman, K. Maltman, G. J. Stephenson, Jr., K. E. Schmidt, and F. Wang, Phys. Rev. C **39**, 1889 (1989).
[6] P. J. Mulders, Phys. Rev. D **26**, 3039 (1982).
[7] A. Pricking, M. Bashkanov, and H. Clement, arXiv:1310.5532 [nucl-ex].
[8] J. Ball *et al.*, Nucl. Phys. A **559**, 489 (1993).
[9] A. de Lesquen *et al.*, Eur. Phys. J. C **11**, 69 (1999).
[10] Y. Makdisi, M. L. Marshak, B. Mossberg, E. A. Peterson, K. Ruddick, J. B. Roberts, and R. D. Klem, Phys. Rev. Lett. **45**, 1529 (1980).
[11] R. Diebold *et al.*, Phys. Rev. Lett. **35**, 632 (1975).
[12] P. Adlarson *et al.*, Phys. Rev. Lett. **112**, 202301 (2014).
[13] C. Bargholtz *et al.*, Nucl. Inst. Methods A **594**, 339 (2008).
[14] H. H. Adam *et al.*, arXiv:nucl-ex/0411038.
[15] M. Haji-Saied *et al.*, Phys. Rev. C **36**, 2010 (1987).
[16] J. Arvieux *et al.*, Nucl. Phys. A **431**, 613 (1984).
[17] D. Mchedlishvili, Internal ANKE Report No. 28, 2013; available at: http://collaborations.fz-juelich.de/ikp/anke/internal_notes/DM_Internal_report_dp.pdf
[18] M. Altmeier *et al.*, Eur. Phys. J. A **23**, 351 (2005).
[19] SAID database, http://gwdac.phys.gwu.edu/; R. A. Arndt, W. J. Briscoe, I. I. Strakovsky, and R. L. Workman, Phys. Rev. C **76**, 025209 (2007).
[20] R. Machleidt, Phys. Rev. C **63**, 024001 (2001).
[21] R. A. Arndt, L. D. Roper, R. A. Bryan, R. B. Clark, B. J. VerWest, and P. Signell, Phys. Rev. D **28**, 97 (1983).
[22] C. R. Newsom *et al.*, Phys. Rev. C **39**, 965 (1989).
[23] J. Ball *et al.*, Nucl. Phys. A **559**, 477 (1993).
[24] J. Arnold *et al.*, Eur. Phys. J. C **17**, 67 (2000).
[25] M. W. McNaughton *et al.*, Phys. Rev. C **48**, 256 (1993); **53**, 1092 (1996).
[26] G. Glass *et al.*, Phys. Rev. C **47**, 1369 (1993).
[27] M. L. Barlett *et al.*, Phys. Rev. C **27**, 682 (1983); **40**, 2697 (1989).
[28] R. A. Arndt, J. S. Hyslop, and L. D. Roper, Phys. Rev. D **35**, 128 (1987).
[29] R. A. Arndt, W. J. Briscoe, I. I. Strakovsky, and R. L. Workman, Phys. Rev. C **74**, 045205 (2006); R. L. Workman, R. A. Arndt, W. J. Briscoe, M. W. Paris, and I. I. Strakovsky, *ibid.* **86**, 035202 (2012).
[30] J. S. Hyslop, R. A. Arndt, L. D. Roper, and R. L. Workman, Phys. Rev. D **46**, 961 (1992).
[31] G. Höhler, πN Newsletter **9**, 1 (1993).
[32] O. Hanstein, D. Drechsel, and L. Tiator, Phys. Lett. B **385**, 45 (1996).
[33] P. W. Lisowski, R. E. Shamu, G. F. Auchampaugh, N. S. P. King, M. S. Moore, G. L. Morgan, and T. S. Singleton, Phys. Rev. Lett. **49**, 255 (1982).
[34] T. J. Devlin *et al.*, Phys. Rev. D **8**, 136 (1973).
[35] V. I. Sharov *et al.*, Eur. Phys. J. C **37**, 79 (2004); **13**, 255 (2000).
[36] F. Lehar *et al.*, Phys. Lett. B **189**, 241 (1987).
[37] J. M. Fontaine *et al.*, Nucl. Phys. B **358**, 297 (1991).
[38] J. Ball *et al.*, Z. Phys. C **61**, 53 (1994).
[39] M. Beddo *et al.*, Phys. Rev. D **50**, 104 (1994).
[40] B. P. Adiasevich *et al.*, Z. Phys. C **71**, 65 (1996).
[41] Y. Terrien *et al.*, Phys. Rev. Lett. **59**, 1534 (1987).
[42] G. Bizard *et al.*, Nucl. Phys. B **85**, 14 (1975).
[43] D. Mchedlishvili *et al.*, Eur. Phys. J. A **49**, 49 (2013), and private communication.
[44] F. Lehar and C. Wilkin, Eur. Phys. J. A **37**, 143 (2008).
[45] C. Wilkin, in *NN and 3N Interactions*, edited by L. Blokhintsev and I. I. Strakovsky (Nova Science, New York, 2014), p. 43.
[46] F. J. Dyson and N.-H. Xuong, Phys. Rev. Lett. **13**, 815 (1964).
[47] M. Gell-Mann, Phys. Lett. B **8**, 214 (1964).
[48] M. Bashkanov, S. Brodsky, and H. Clement, Phys. Lett. B **727**, 438 (2013).
[49] H. Huang, J. Ping, and F. Wang, Phys. Rev. C **89**, 034001 (2014).
[50] X. Q. Yuan, Z. Y. Zhang, Y. W. Yu, and P. N. Shen, Phys. Rev. C **60**, 045203 (1999).
[51] F. Huang, Z. Y. Zhang, P. N. Shen, and W. L. Wang, arXiv:1408.0458 [nucl-th].
[52] A. Gal and H. Garcilazo, Phys. Rev. Lett. **111**, 172301 (2013).
[53] A. Gal and H. Garcilazo, Nucl. Phys. A **928**, 73 (2014).
[54] P. Adlarson *et al.*, arXiv:1409.2659 [nucl-ex].
[55] D. V. Bugg, Eur. Phys. J. A **50**, 104 (2014).
[56] F. Kren *et al.*, Phys. Lett. B **684**, 110 (2010); **702**, 312 (2011); arXiv:0910.0995v2 [nucl-ex].
[57] T. Skorodko *et al.*, Phys. Lett. B **695**, 115 (2011).
[58] T. Skorodko *et al.*, Eur. Phys. J. A **47**, 108 (2011).
[59] T. Skorodko *et al.*, Phys. Lett. B **679**, 30 (2009).